## Supplemental data for "A lone spike in blood glucose can enhance the thrombo-inflammatory response in cortical venules"

### Methods for concurrent in vivo imaging and laser induction of intravascular blood platelet aggregates

Live images of mouse cerebral vasculature were obtained with a system of local design in which a two-photon laser scanning microscope incorporates a beam line from an amplified 100-femtosecond pulsed laser[1].

***Cojoining of beams.*** The beam line for imaging by two-photon microscopy utilizes low-energy, 100-fs pulses at a repetition rate of 76-MHz and a center wavelength of 840 nm. This beam is generated by a commercial fiber laser oscillator (Chameleon Discovery; Coherent Inc.). It is naturally polarized. The beam line for laser induction of an intravascular thrombus by targeted irradiation utilizes high-energy, 100-fs pulses at a repetition rate of 1-kHz and a center wavelength of 805 nm. This beam is generated by a commercial combined seed laser and multi-pass amplifier (Astrella; Coherent Inc.). This beam too is naturally polarized. The imaging beam and the ablation beam were combined before the microscope objective with a polarizing beam splitter. A half-wave plate (λ/2) for each beam rotates the polarization of the amplified pulses to lie vertical and that of the laser oscillator to lie horizontal, so that both beams are perpendicular to each other yet lie of different polarization axes of the polarizing beam splitter (**Figure 1C**). These beams pass through the objective; we used a 0.95-NA, 25X, water-dipping objective (Leica).

***Cofocusing of beams*** .We centered the ablation beam within the area that is raster-scanned by the imaging beam so that damage occurred at the center of the imaging field. We further focused the two beams to the same focal plane by slight alteration of the vergence of the ablation beam.

***Gating and energy control***. The energy per pulse of the ablation beam was attenuated with successive sets of half-wave plates, polarizing beam splitters, and beam dumps. The number of pulses was controlled by a mechanical shutter (Uniblitz LS3Z2 shutter and VMM-D1 driver; Vincent).

1 Tsai, P. S. & Kleinfeld, D. in *Methods for In Vivo Optical Imaging, 2nd edition* (ed R. D. Frostig) 59-115 (CRC Press, 2009).

**Supplemental Figure 1. STZ induced hyperglycemia increases susceptibility to laser-induced vascular disruption**.

**(A)** Blood glucose level measurements (6 mice) over 120 minutes after injection of saline (control) in STZ mice followed by use of the same animals after injection of insulin. The bars are the SEM.

**(B)** Study design.

(**C**) Schematic of set-up and image of surface vasculature of mouse cortex; arrow indicates branch of superior cerebral vein targeted with 0.2 μJ, 0.5 μJ, and 1.0 μJ laser energy, following treatment with saline (upper vein) or insulin (lower vein).

(**D**) Representative images of platelet (green) and serum (red) fluorescence in cortical veins targeted by 0.2 μJ, 0.5 μJ, and 1.0 μJ laser pulses, 30 s post laser-induced vascular disruption, in STZ mice treated with saline and STZ mice treated with insulin. Site of focal damage is marked with yellow circle, along with vein outline in some images.

(**E**) Effects of varying laser energy on the time course of laser-induced thrombi and blood extravasation. Each curve is generated from the average change in vein fluorescence relative to baseline values. We used 9 mice total. All 9 mice received a $1^{st}$ injection of saline and each of 3 veins in each animal were irradiated at 0.2 μJ, 0.5 μJ, and 1.0 μJ. Then 6 of the 9 mice received a $2^{nd}$ injection of insulin (1 unit/kg) and each of 3 additional veins in each animal were irradiated at 0.2 μJ, 0.5 μJ, and 1.0 μJ. Further, 3 of the 9 mice received a $2^{nd}$ injection of saline and each of 3 additional veins in each animal were irradiated at 0.2 μJ, 0.5 μJ, and 1.0 μJ. Data was smoothed with 2.4 s median filter. We determined the effect of insulin suppression of susceptibility to laser-induced damage for the first 100 s after the pulse by calculating the rank order (one sided non-paired Wilcoxon) for STZ + insulin relative to STZ alone for each energy level as well as the ratio for STZ + insulin relative to STZ + saline for each energy level. NS - not significant or $p > 0.05$.

(**F**) Representative three-dimensional reconstructions of thrombi (green) within vasculature (red), collected 600 s post laser-induced vascular disruption.

(**G**) Thrombi volumes at 600 s post laser-induced vascular disruption. Same veins as in panel D. The red bar is the mean (40 ± 9 pl for STZ; 3.6 ± 0.7 pl for STZ+insulin; 32 ± 4 pl for STZ+saline). For STZ only the value significantly differs from the baseline value of **Figure 1G** ($p < 1.1 \times 10^{-4}$). For STZ + insulin the value does not differ from the baseline value ($p = 0.97$). For STZ + saline the value significantly differs from the baseline value ($p < 1.3 \times 10^{-5}$) and is equivalent to the STZ only value ($p = 0.55$).

(**H**) Thrombus volume fractions; reanalysis of the data in panel F. The red bar is the mean (0.22 ± 0.05 for STZ; 0.035 ± 0.006 for STZ+insulin; 0.24 ± 0.09 for STZ+saline). For STZ only the value significantly differs from the baseline value of **Figure 1H** ($p < 0.01$). For STZ + insulin the value does not differ from the baseline value ($p = 0.27$). For STZ + saline the value significantly differs from the baseline value ($p < 0.02$) and is equivalent to the STZ only value ($p = 0.80$).

**Supplemental Figure 2. Obesity related type 2 hyperglycemia increases susceptibility to vascular disruption.**

(**A**) Body mass measurements in *db/db* in comparison to wild type control mice (8 *db/db* and 8 WT mice); the differences are significant with $p < 10^{-12}$. The red bar is the mean; 49.8 ± 1.0 g for *db/db* (mean ± SD) for 25.8 ± 0.5 g for WT.

(**B**) Blood glucose level measurements in *db/db* in comparison to wild type control mice; the differences are significant with $p < 10^{-7}$. The red bar is the mean (137 ± 9 mg/dl for control; 351 ± 24 mg/dl for *db/db*). Same mice as in panel A.

(**C**) Study design.

(**D**) Schematic of set-up and image of surface vasculature of mouse cortex; arrow indicates branch of superior cerebral vein targeted with 1.0 μJ laser energy.

(**E**) Representative fluorescent images of platelet (green) and serum (red) fluorescence in cortical surface veins, before and 30 s and 200 s post laser-induced vascular disruption using 1.0 μJ laser pulses, in wild type control mice in comparison to *db/db* mice. Focal region of the excitation spot is highlighted by the yellow circle.

(**F**) Effects of 1.0 μJ laser pulses on the time course of laser-induced platelet-rich thrombi and serum extravasation. Each curve is generated from the average change in vein fluorescence relative to baseline values. We used 5 *db/db* mice with one vein targeted per mouse and 6 WT mice with one vein targeted per mouse, for a grand total of 11 mice. Data was smoothed with 2.4 s median filter; the light red bands are the 1 SD intervals. The changes for *db/db* mice are significant relative to control animals for both platelets (one-sided Wilcoxon for initial 100 s after pulse) and serum extravasation (near steady-state, i.e., 300 - 400 s after pulse).

(**G**) Representative three-dimensional reconstructions of thrombi (green) within vasculature (red), collected 600 s post laser-induced vascular disruption.

(**H**) Thrombi volumes at 600 s post laser-induced vascular disruption. Same veins as in panel D. The red bar is the mean (1.6 ± 0.6 pl for control; 15 ± 4 pl for *db/db*). For control mice the value does not differ from the baseline value of **Figure 1G** ($p = 0.17$). For *db/db* mice the value is significantly different from the baseline value ($p < 0.0016$).

(**I**) Thrombus volume fractions; reanalysis of the data in panel F. The red bar is the mean (0.030 ± 0.008 for control; 0.25 ± 0.08 for *db/db*). For control mice the value does not differ from the baseline value of **Figure 1H** ($p = 0.16$). For *db/db* mice the value is significantly different from the baseline value ($p < 0.019$).

**Supplemental Figure 3. Vein diameter measurements.**

(**A**) Diameter measurements for veins included in Figure 1 G/H.

(**B**) Diameter measurements for veins included in Figure 3 F/G.

(**C**) Diameter measurements for veins included in Figure 4 F/G.

(**D**) Diameter measurements for veins included in Figure 5 F-I.

(**E**) Diameter measurements for veins included in Figure 6 F/G.

**Supplemental Figure 4. Histological analysis of additional amplified pulsed laser perturbed veins .**

**(A)** Fluorescent images of a lesioned vein from 3 serial sections. Left panels illustrate luminal accumulations of platelets labeled in vivo with CD41 antibody. Platelet aggregation identifies in vivo vessel injury. Right panels illustrate immunoreactivity for markers of activated endothelium.

**(B)** Fluorescent images of nontargeted veins in same section as lesioned vein. Veins demonstrates scant or no CD41. As these preparations are not exsanguinated for brain harvesting, it is not surprising that circulating platelets are variably trapped in vessels. Right panels illustrate the negligible immunoreactivity to ICAM-1. Collagen-IV, and VWF in vessels on the same section as in panel A.

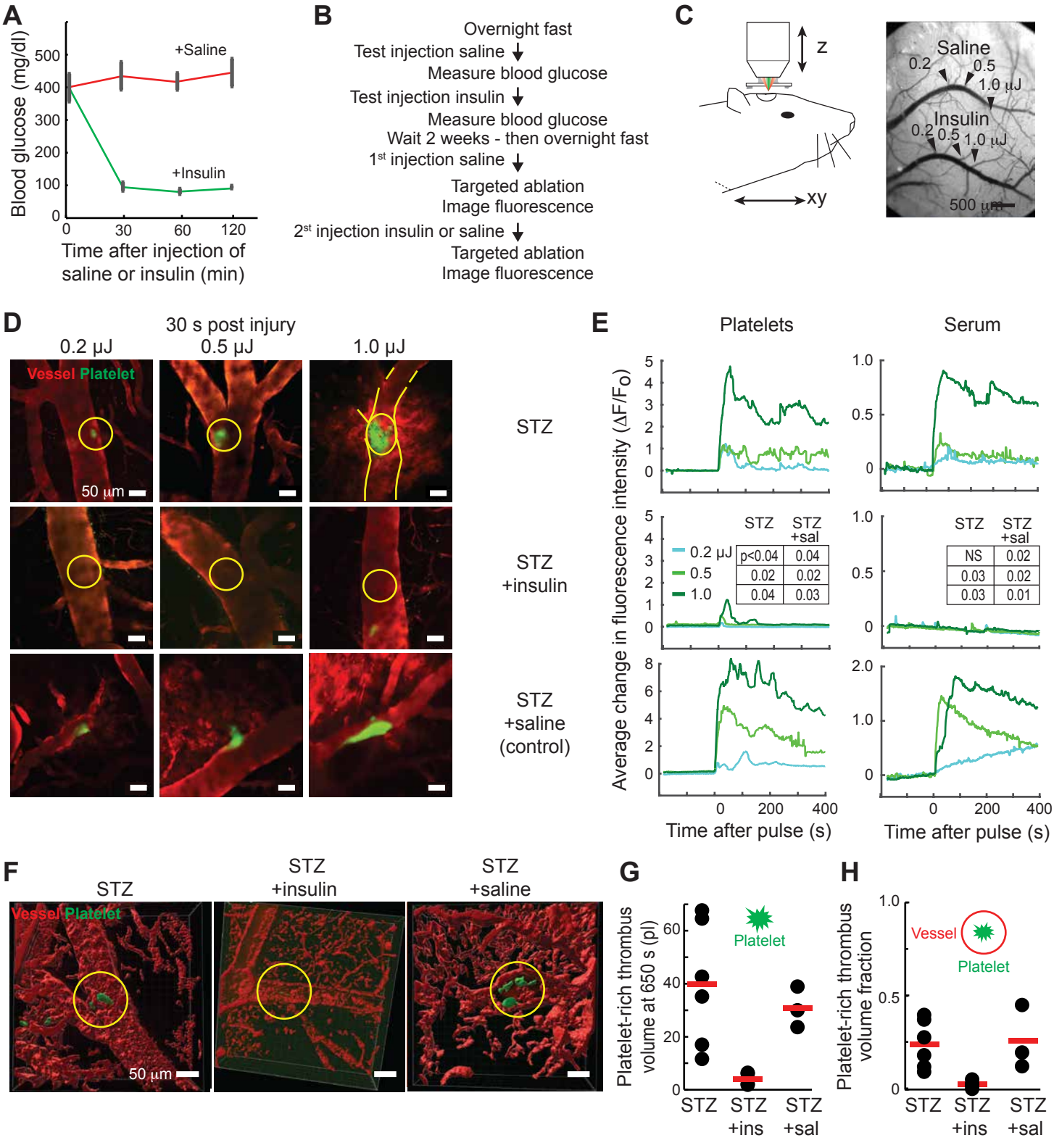


Supplemental Figure_1. Shaked et al.

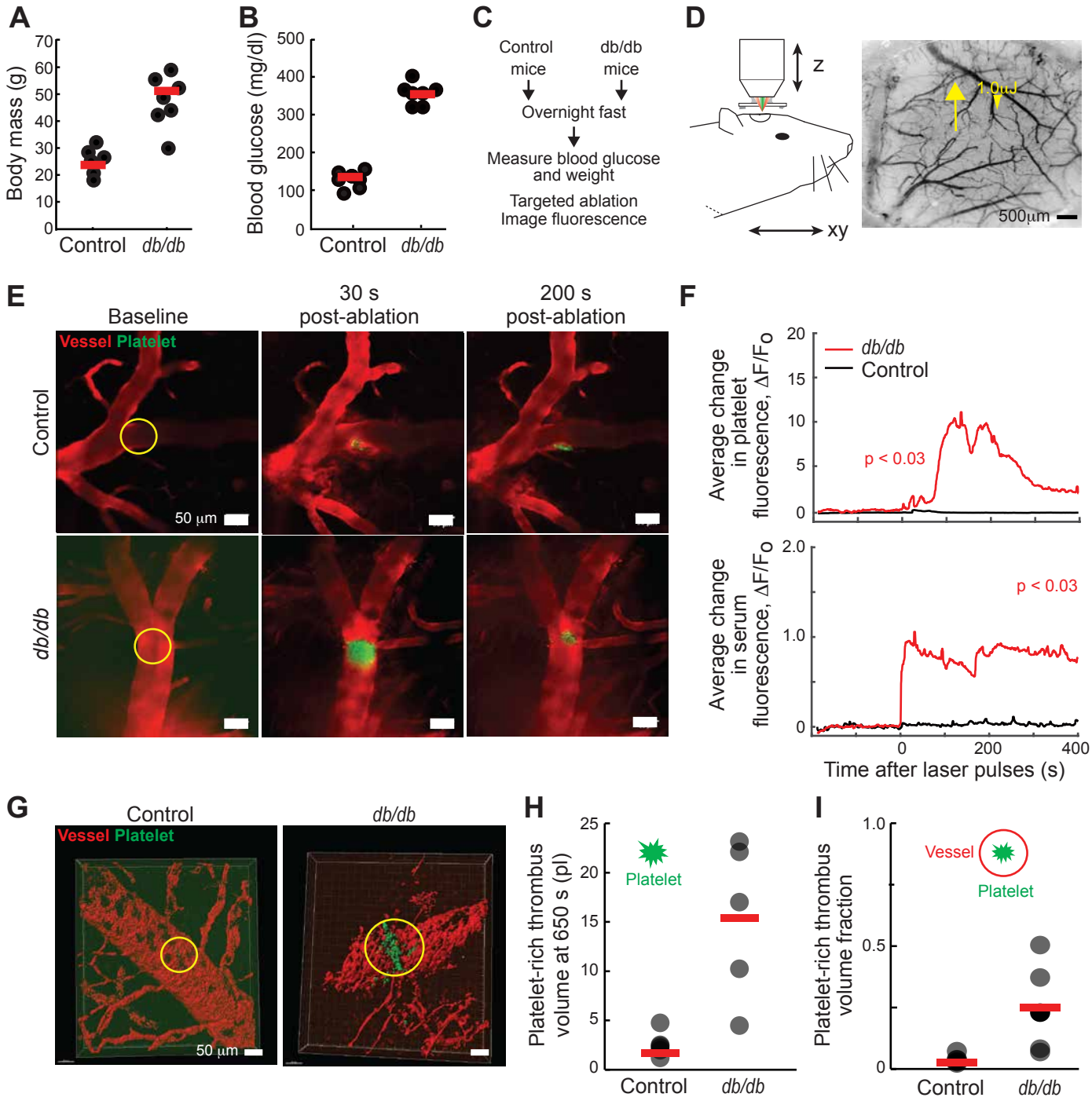


Supplemental Figure_2. Shaked et al.

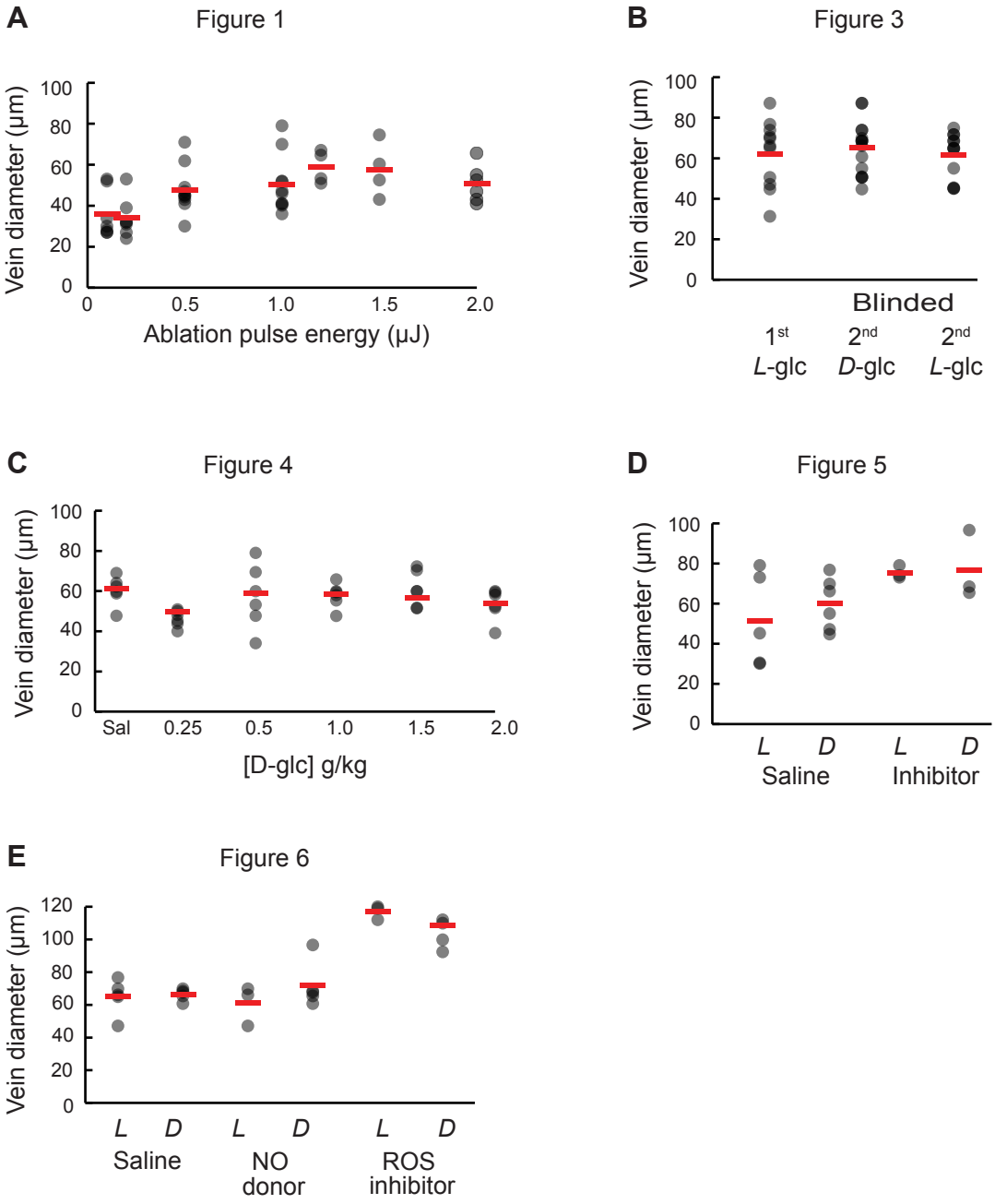


Figure Suppl 3 Shaked et al.

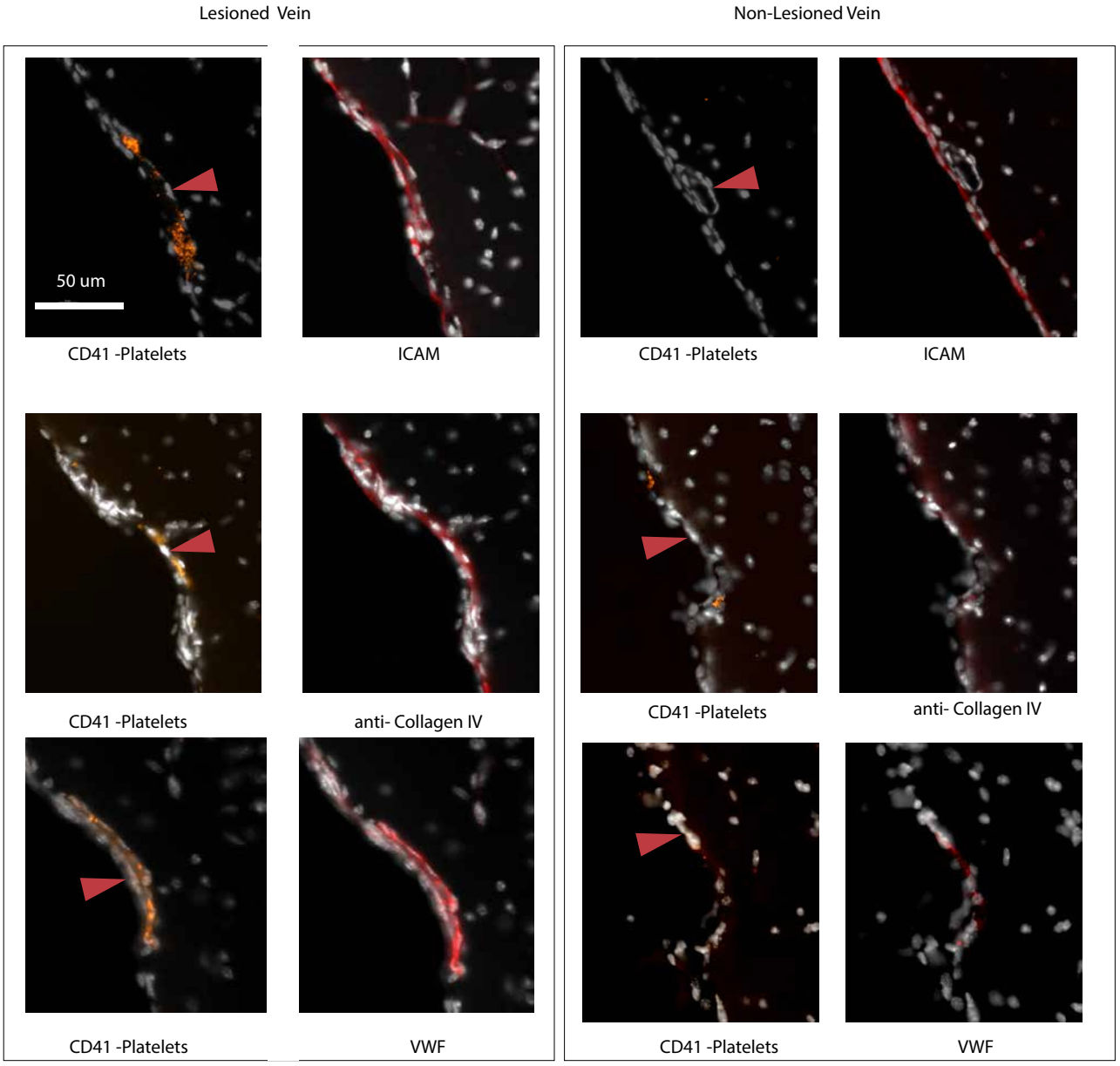


Supplemental Figure_4. Shaked et al.